https://doi.org/10.5194/egusphere-2023-451
Preprint. Discussion started: 24 April 2023

Understanding variations in downwelling longwave radiation using Brutsaert's equation

Yinglin Tian[1,2], Deyu Zhong[1], Sarosh Alam Ghausi[2,3], Guangqian Wang[1], Axel Kleidon[2]

[1]State Key Laboratory of Hydroscience and Engineering, Department of Hydraulic Engineering, Tsinghua University, 100084 Beijing, China.
[2]Biospheric Theory and Modelling, Max Planck Institute for Biogeochemistry, 07701 Jena, Germany
[3]International Max Planck Research School on Global Biogeochemical Cycles (IMPRS-gBGC), 07701 Jena, Germany

Correspondence to: Axel Kleidon (akleidon@bgc-jena.mpg.de)

Abstract

A dominant term in the surface energy balance and central to global warming is downwelling longwave radiation (R_{ld}). It is influenced by radiative properties of the atmospheric column, in particular by greenhouse gases, water vapour, clouds and differences in atmospheric heat storage. We use the semi-empirical equation derived by Brutsaert (1975) to identify the leading terms responsible for the spatio-temporal climatological variations in R_{ld}. This equation requires only near-surface observations of air temperature and humidity. We first evaluated this equation and its extension by Crawford and Duchon (1999) with observations from FLUXNET, the NASA-CERES dataset , and the ERA5 reanalysis. We found a strong agreement with r^2 ranging from 0.87 to 0.99 across the datasets for clear-sky and all-sky conditions. We then used the equations to show that diurnal and seasonal variations in R_{ld} are predominantly controlled by changes in atmospheric heat storage. Variations in the emissivity of the atmosphere form a secondary contribution to the variation in R_{ld}, and are mainly controlled by anomalies in cloud cover. We also found that as aridity increases, the contributions from changes in emissivity and atmospheric heat storage tend to offset each other (-40 W m^{-2} and 20-30 W m^{-2}, respectively), explaining the relatively small decrease in R_{ld} with aridity (-(10-20) W/m^{-2}). These equations thus provide a solid physical basis for understanding the spatio-temporal variability of surface downwelling longwave radiation. This should help to better understand and interpret climatological changes, such as those associated with extreme events and global warming.

https://doi.org/10.5194/egusphere-2023-451
Preprint. Discussion started: 24 April 2023

1 Introduction

In the global mean surface energy budget, downward longwave radiation (R_{ld}) is the dominant term (333 W/m^2), contributing more than twice as much energy as absorbed solar radiation (161 W/m^2) (Trenberth et al. 2009). This dominance holds over all regions in the climatological mean, although there are some clear variations in space and time (Figure 1). It is central to global warming, reflecting the greenhouse effect of the atmosphere (Held and Soden 2000), and its variations have been suggested to be the main contributor to some regional warming amplifications, such as in the Arctic (Lee et al. 2017) and the Tibetan Plateau (Su et al. 2017). Therefore, it is important to understand the main sources of variations in this surface energy balance term, which can be seen in Figure 1.

The flux of downwelling longwave radiation is influenced by the radiative properties of the entire atmospheric column, i.e., water vapour, clouds and greenhouse gases, but also by the heat stored in the atmosphere, i.e., the temperature at which radiation is emitted back to the surface. To obtain an estimate of this flux, Brutsaert (1975) used functional expressions for the typical temperature and humidity profiles of the lower troposphere together with radiative transfer equations and semiempirical relationships of the absorptivity by water vapor, integrated these vertically, and expressed the resulting flux R_{ld} in terms of near-surface air temperature and water vapour pressure for clear-sky conditions. He thereby derived a semi-empirical equation for R_{ld} for an effective clear sky emissivity (ε_{cs}) and the corresponding flux of downwelling longwave radiation ($R_{ld,cs}$):

$$\varepsilon_{cs} = 1.24(e_a/T_a)^{1/7}, \tag{1}$$

$$R_{ld,cs} = \varepsilon_{cs}\sigma T_a{}^4. \tag{2}$$

where σ is Stefan–Boltzmann constant (σ = 5.67 10^{-8} W m^{-2} K^{-4}), e_a is the water vapor pressure and T_a is the 2m air temperature. The latter two meteorological variables can easily be obtained or inferred from weather stations, so that the downwelling flux of longwave radiation can be estimated from weather station observations.

This equation was later extended to all-sky conditions that include the effects of cloud cover, among which Crawford and Duchon (1999) is a common extension (Alados et al. 2012; Duarte et al. 2006; Flerchinger et al. 2009). This extension diagnoses cloud cover fraction (f_c) as the fraction of incoming solar radiation at the surface (R_s) in relation to the potential solar radiation ($R_{s,pot}$), that is, the incoming flux at the top of the atmosphere. The emissivity for all-sky conditions, ε, is then calculated as the mix of the emissivities of clear-sky conditions (Eqn. (1), weighted by the cloud-free proportion, $1 - f_c$) and clouds with an emissivity of $\varepsilon_c = 1$ (weighted by the cloud fraction f_c). Using this emissivity, the estimation of downwelling longwave radiation is then done by

$$f_c = 1 - R_s/R_{s,pot}, \tag{3}$$

$$\varepsilon = f_c + (1 - f_c)\varepsilon_{cs}, \tag{4}$$

$$R_{ld} = \varepsilon\sigma T_a{}^4 \tag{5}$$

Previous studies have already verified this estimate to have a very good agreement with site measurements (Duarte et al. 2006; Hatfield et al. 1983), especially when the temperature is higher than 0℃ (Aase and Idso 1978; Satterlund 1979). Other studies have worked to calibrate and modify this estimate further to different regions (Malek 1997; Sridhar and Elliott 2002).

This expression for downwelling longwave radiation R_{ld} given by Eqn. (5) allows us to quantify the different contributions by cloud cover, f_c, water vapor concentrations, e_a (as a measure of the total water vapor content of the atmospheric column), and air temperature, T_a (as a proxy for the total atmospheric heat storage within the column). With this, we can then attribute variations in R_{ld} to their physical causes.

https://doi.org/10.5194/egusphere-2023-451
Preprint. Discussion started: 24 April 2023

Here, our aim is to first evaluate this estimate for downwelling longwave radiation with current global datasets at the continental scale. These variations are illustrated using the NASA-CERES (EBAF 4.1) dataset (Loeb et al., 2018; Kato et al., 2018, NASA/LARC/SD/ASDC 2017) and the NASA-CERES Syn1deg dataset (Doelling et al., 2013, 2016) in Figure 1 and are compared to variations in solar radiation. It can be seen that the climatological distribution of R_{ld} is mostly associated with latitudes, while also presenting some zonal variations, e.g., across western and eastern North America. In comparison, the seasonal cycle of R_{ld} is less determined by latitudes (Fig. 1b). It has a larger magnitude over land than over oceans, over arid regions than humid regions, and over cold regions more than over warm ones. Although studies have revealed a close correlation between the variation of R_{ld} and other factors like air temperature, water vapor, and CO_2 concentration (Wang and Liang 2009; Wei et al. 2021), here we go beyond correlations and rather attribute these variations to the different terms in Eqns. (1)-(5) that represent different radiative properties affecting R_{ld}.

To figure out the dominant driver for these spatiotemporal variations, we decompose changes in R_{ld} into its components: cloud cover, f_c, heat storage changes of atmosphere as reflected by 2m air temperature, T_a, and air humidity, e_a, by performing the differentiation of these equations. We show that heat storage changes predominantly shape the diurnal range and seasonal cycle of R_{ld}, while cloud cover variations play a second role in most cases. In addition, the temporal variations of R_{ld} are less over the ocean than over land, and less during winter than summer. On the other hand, the spatial variations of R_{ld} from arid to humid regions is relatively small, which we will show is due to a compensating effect of corresponding changes in atmospheric emissivity and heat storage.

Our paper is organized as follows: After briefly describing the datasets used in our evaluation in Section 2, we first the estimate of R_{ld} from these equations at the global scale, using multiple datasets in Section 3.1. After showing that the annual-mean and large-scale variations are well captured, we then use the equations to decompose the temporal variations of R_{ld} in terms of its mean spatial and temporal variations and relate these to their causes in Section 3.2. The spatial variations of R_{ld} are then further discussed in Section 3.3 in terms of its relationship with aridity. We then close with a brief summary and broader implications.

2 Datasets

To test R_{ld} estimates, we use FLUXNET observations (Pastorello et al. 2020, half-hourly values, 189 sites, see Table S1 for details), the NASA CERES satellite-based radiation dataset (Doelling et al., 2013, 2016, monthly means, covering years 2001 to 2018), and the ERA5 reanalysis dataset (Hersbach et al. 2018, monthly means, covering years 1979 to 2021).

For each dataset, T_a, e_a, and f_c are needed as inputs for Eqs. (1)-(5), while R_{ld} data is used for the comparison. For FLUXNET and ERA5, water vapor pressure, e_a, is not directly given. It is calculated from the water vapor deficit (VPD, FLUXNET) or dewpoint temperature (T_{dew}, ERA5) using Monteith and Unsworth (2008):

$$e_a = 6.1079 \times \exp\left(17.269 T_{dew}/(237.3 + T_{dew})\right), \quad (6)$$

$$e_a = 6.1079 \times \exp\left(17.269 T_a/(237.3 + T_a)\right) - VPD, \quad (7)$$

Since the NASA-CERES dataset includes cloud cover, f_c, this is used directly in the estimation instead of using Eq. (3), together with e_a from ERA5 and T_a from the CPC Global Unified Temperature dataset (CPC Global Unified Temperature).

For the analysis of the spatial variations of R_{ld} along water availability, we use the aridity index (AI $= \frac{R}{LP}$) (Budyko 1958; UNCOD 1977). This index is calculated using the mean annual net radiation (R) taken from the NASA-CERES dataset, the mean annual net precipitation (P) taken from the CPC Global Unified Gauge-Based Analysis of Daily Precipitation data (Chen et al. 2008 and Xie et al. 2007, CPC Global Unified

https://doi.org/10.5194/egusphere-2023-451
Preprint. Discussion started: 24 April 2023

Gauge-Based Analysis of Daily Precipitation), and a latent heat of vaporization for water of $L = 2260$ kJ/kg. A larger value of *AI* indicates stronger aridity.

3 Results and discussion

3.1 Comparison to observed, satellite, and reanalysis data

We first compared the estimates of R_{ld} at a point-by-point basis separately for clear-sky and all-sky conditions using Eqns. (2) and (5), respectively. This comparison is shown in Figure 2 using FLUXNET, CERES, and ERA5 data. The estimates correlate very well with r^2 of 0.92 and 0.87 for clear-sky and all-sky conditions, respectively, and RMSE values of 18.2 and 24.6 W m^{-2}. The slope of the linear regressions between the estimated and observed R_{ld} for FLUXNET are 1.03 and 1.02, with most data points being concentrated around the 1:1 line (Figs. 2a and 2b). Note that for all-sky conditions, the agreement is slighty less good, with a lower correlation coefficient and a larger RSME. The agreement with the NASA-CERES and ERA5 datasets are even better, with higher correlation coefficients and lower RSME.

Despite this high level of agreement of the estimates, we can see some systematic biases in the estimates for R_{ld}. These can be seen in Figure 3, which shows the spatial distribution of these biases for the NASA-CERES and ERA5 comparison. For clear-sky conditions, there appears to be a general underestimation in the high latitudes and, to some extent, in arid regions (Figs. 3a and 3c). This bias can be attributed to biases in the equations used here. Brutsaert (1975) already described that for very low temperatures and in arid conditions, there are better parameter values than those used in Eq. 1, with a larger coefficient than 1.24 and a different exponent. The biases seen in Figure 3 are nevertheless notably smaller than the seasonal variations shown in Figure 1.

The biases for all-sky conditions are typically larger and generally positive, implying an overestimate except for the extremely cold and dry regions (Figs. 3b and 3d). This indicates that the effect of cloud cover is probably more complex than the simple accounting expressed in Eqns. (4) and (5). However, the biases are also small compared to the seasonal variations.

Overall, this evaluation shows that the expressions given by Eqns. (1) - (5) are very well suited to describe the spatiotemporal variations of R_{ld} for current climatological conditions.

3.2 Attribution of diurnal and seasonal variations

We next use Eqns. (1) - (5) to attribute temporal variations of R_{ld} to their physical causes. To do so, we can express changes ΔR_{ld} as a function of changes in water vapor, Δe_a, cloud cover, Δf_c, and air temperature, ΔT_a. The functional dependence is derived from the equations by differentiation and applying the chain rule. In a first step, we express a change ΔR_{ld} by the partial contributions $\Delta R_{ld,\varepsilon}$ and $\Delta R_{ld,T}$, that are due to changes in emissivity, $\Delta\varepsilon$, and due to changes in atmospheric heat storage that are associated with a change in air temperature ΔT_a:

$$\Delta R_{ld} = \Delta R_{ld,\varepsilon} + \Delta R_{ld,T} = \frac{\partial R_{l,d}}{\partial \varepsilon}\Delta\varepsilon + \frac{\partial R_{l,d}}{\partial T_a}\Delta T_a = \sigma\overline{T_a}^4\Delta\varepsilon + 4\sigma\bar{\varepsilon}\overline{T_a}^3\Delta T_a. \tag{8}$$

The contribution $\Delta R_{ld,\varepsilon}$ is further decomposed into contributions $\Delta R_{ld,f_c}$ and $\Delta R_{ld,e_a}$ due to variations in clouds, Δf_c, and air humidity, Δe_a . Note that the contribution of a change ΔT_a to $\Delta R_{ld,\varepsilon}$ is relatively small and is thus neglected here. We obtain:

https://doi.org/10.5194/egusphere-2023-451
Preprint. Discussion started: 24 April 2023

$$\Delta R_{ld,\varepsilon} = \sigma\, \overline{T_a}^4 \Delta\varepsilon \approx \frac{\partial\varepsilon}{\partial f_c}\Delta f_c + \frac{\partial\varepsilon}{\partial e_a}\Delta e_a$$
$$= \sigma\overline{T_a}^4 \times \left(1 - 1.24\,\overline{\left(\frac{e_a}{T_a}\right)^{\frac{1}{7}}}\right)\Delta f_c + \sigma\overline{T_a}^4 \times \frac{1.24}{7}\frac{(1-\overline{f_c})}{(\overline{e_a})^{\frac{6}{7}}(\overline{T_a})^{\frac{1}{7}}}\Delta e_a, \tag{9}$$

We next applied this approach to the diurnal deviations ΔR_{ld} from the daily mean using the FLUXNET dataset. This decomposition is shown in Figure 4 in aggregated form across the FLUXNET sites for whole year (Fig. 4a), the Northern hemisphere summer (Fig. 4b) and winter seasons (Fig. 4c). The diurnal variations of about ± 20 W m^{-2} are primarily caused by diurnal changes in air temperature, while variations in emissivity play practically no role. Diurnal changes in air temperature reflect variations in heat storage of the atmospheric boundary layer. This is consistent with the notion that diurnal variations in solar radiation over land are buffered primarily by the lower atmosphere, rather than below the surface as it is the case for open water bodies and the ocean (Kleidon and Renner 2017). Since most of the stations in the FLUXNET dataset are located in the midlatitudes of the Northern hemisphere, the variations are consistently larger in summer due to the greater solar input (Fig. 4b) than in winter (Fig. 4c).

Figure 5 shows the same kind of decomposition, but for seasonal variations in R_{ld} in the NASA CERES dataset. The aggregation to the global scale across land and ocean is also shown in Fig. 5e-h. For the decomposition in Fig. 5e-h, the deviations are calculated as the difference of the monthly means to the annual mean. Generally, areas with relatively low annual-mean R_{ld}, e.g. the high latitude regions of North America and northeastern Eurasia, have the largest seasonal cycle (Fig. 1). The decomposition shows that this variation is mostly due to the seasonal variation in atmospheric heat storage ($\Delta R_{ld,T}$), although it is to some extent amplified by the contribution due to emissivity changes ($\Delta R_{ld,\varepsilon}$). Seasonal variations in emissivity play a greater role in changing R_{ld} in tropical areas, and this is predominantly due to cloud cover changes (Fig. 5c). The contribution by changes in water vapor is generally much smaller and does not vary much across regions (Fig. 5d).

Figs. 5e - h show that the seasonal variations of R_{ld} is generally less over the ocean than on the land, an effect that can also be seen in Fig. 1. The decomposition shows that these variations are mostly caused by changes in atmospheric heat storage, with a slight modulation by emissivity changes. This can, again, be largely explained by the effect described above for the diurnal variations (Kleidon and Renner 2017). Because solar radiation penetrates the transparent water bodies over marine areas, its variations are buffered below the surface, and not within the atmosphere. These variations are then reflected in seasonal changes in sea surface temperature. On land, however, seasonal heat storage changes below the surface are generally quite small, so that most variations take place in the lower atmosphere, which then alter R_{ld}.

These results show very similar patterns in the ERA5 dataset (Fig. S2).

In summary, what our decomposition shows is that most temporal variations in R_{ld} in current, climatological conditions are explained by heat storage changes within the lower atmosphere.

3.3 Attribution of geographic variations with aridity

Last, we applied the decomposition to the climatological variations in R_{ld} along differences in mean water availability. Water availability was characterized by Budyko's aridity index (AI), with values AI < 1 representing humid regions, and larger values reflecting increased ariditiy. Here, the deviations ΔR_{ld} are calculated with respect to the global annual mean. The different contributions to the deviations are shown in Fig. 6, as well as the delineation along the aridity index (Figs. 6e - h).

https://doi.org/10.5194/egusphere-2023-451
Preprint. Discussion started: 24 April 2023

The decomposition of the spatial distribution of the climatological means shows that the variations are largely caused by differences in atmospheric heat storage as well (Fig. 6a). The contribution due to variations in emissivity has a much smaller magnitude (Fig. 6b), and is dominated by changes in cloud cover (Fig. 6c). Changes in water vapor appear to influence R_{ld} mostly in the humid tropics (Fig. 6d). The results for the ERA5 reanalysis dataset show the same patterns (Fig. S1).

These variations are evaluated with respect to the aridity index in Figs. 6e - h. While there is a large spread, as seen in the quantiles, there is a small, but consistent trend towards lower values of R_{ld} in more arid regions, with a magnitude of about 20 W m^{-2} (black dashed line in Figs. 6e and 6g). We also notice a shift in the contributions, with emissivity contributing less and atmospheric heat storage contributing more with increased values of AI. The changes in emissivity is mostly caused by reductions in cloud cover, as shown by the orange lines in Figs. 6f and h, and amounts to around -40 W m^{-2} over the range shown in the Figure. This decrease in cloud cover can be attributed to the common presence of high-pressure systems in subtropical areas (Zampieri et al. 2009). The decreasing contribution by lower cloud cover is compensated for by an increased contribution of about +20 W m^{-2} by atmospheric heat storage that is caused by the generally warmer mean temperatures in arid regions. This compensation is also seen in the ERA5 data (Figs. 6g and 6h), with magnitudes of -40 W m^{-2} and +30 W m^{-2} respectively.

Taken together, these trends imply that, again, the climatological variations in R_{ld} are also dominated by differences in atmospheric heat storage. A small, but consistent change can be seen in the contributions along the aridity index, with the contribution by emissivity due to cloud cover becoming lower while the contribution by atmospheric heat storage increases as regions become drier.

4.Summary and Conclusions

We found that the semiempirical equations of Brutsaert (1975) and Crawford and Duchon (1999) work very well to estimate the downwelling flux of longwave radiation by comparing these to estimates from observation, satellite, and reanalysis datasets. We then showed that one can use these equations to decompose this flux into different components, and relate changes to differences in cloud cover, water vapor, and atmospheric heat storage. We found that most changes in downwelling longwave radiation are caused by differences in atmospheric heat storage that are reflected in differences in air temperature.

These equations can then be applied to different aspects of climate research. For instance, the values of downwelling longwave radiation are often missing in FLUXNET data (Table S2), and these equations can be used to fill the gaps with air temperature and humidity observations. We can also use these equations to better understand the physical mechanisms for temperature change due to extreme events. For instance, Park et al. (2015) and Alekseev et al. (2019) found that an enhancement of downwelling longwave radiation in the Arctic is found to be preceded by the advection of moisture and heat. The equations by Brutsaert (1975) and Crawford and Duchon (1999) can then be used to quantify the individual contributions by the advection of heat and moisture (Tian et al. 2022). Another example is the attribution of differences in global warming magnitudes across humid and arid regions. Du et al. (2020) used these equations to explain why global warming was stronger during clear-sky conditions in observations in China due to the greater sensitivity of clear-sky emissivity to a change in water vapor. This was then used to explain the observed, stronger global warming in the arid regions of China, which have less clouds and a higher frequency of clear-sky conditions than the humid regions. While the empirical coefficient of 1.24 in Eq. (1) may change due to emissivity changes from greenhouse gases other than water vapor, this formulation can nevertheless provide a useful basis.

We conclude that the equations by Brutsaert (1975) and Crawford and Duchon (1999) are still very useful to advance our understanding of surface temperature changes. Our evaluation has shown how well these equations estimate this flux, and our application to the decomposition of different contributions has shown its utility to understand the causes for its variation. These equations should help us to better understand aspects of climate variability, extreme events, and global warming, linking these to the mechanistic contributions by downwelling longwave radiation.

https://doi.org/10.5194/egusphere-2023-451
Preprint. Discussion started: 24 April 2023

Acknowledgments

This research is supported by the National Natural Science Foundation of China (52209026) and the Second Tibetan Plateau Scientific Expedition and Research Program (grant no. 2019QZKK0208). This research resulted from a research stay of YLT in AK's research group. This stay was supported by China Scholarship Council as No. 202106210161. AK and SAG acknowledge funding from the Volkswagen Stiftung through the ViTamins project.

Author contributions

YLT, SAG, and AK conceived and designed the analysis, with inputs from DZ and GW. YLT performed the analysis and discussed the results with all authors. YLT and AK wrote the paper.

Competing interests

The contact author has declared that none of the authors has any competing interests.

Data availability

The data used in this study was downloaded from the links provided with the references. No new data was created.

References

Aase, J. K., and S. B. Idso, 1978: A comparison of two formula types for calculating long-wave radiation from the atmosphere. Water Resources Research, 14, 623-625. https://doi.org/10.1029/WR014i004p00623

Alados, I., I. Foyo-Moreno, and L. Alados-Arboledas, 2012: Estimation of downwelling longwave irradiance under all-sky conditions. International Journal of Climatology, 32, 781-793. https://doi.org/10.1002/joc.2307

Alekseev, G., S. Kuzmina, L. Bobylev, A. Urazgildeeva, and N. Gnatiuk, 2019: Impact of atmospheric heat and moisture transport on the Arctic warming. Int. J. Climatol., 39, 3582–3592, https://doi.org/10.1002/joc.6040.

Budyko, M. I. (1958) The Heat Balance of the Earth's Surface, trs. Nina A. Stepanova, US Department of Commerce, Washington, D.D., 259 p.

Brutsaert, W., 1975: On a derivable formula for long-wave radiation from clear skies. Water Resources Research, 11, 742-744. https://doi.org/10.1029/WR011i005p00742 .

Crawford, T. M., and C. E. Duchon, 1999: An Improved Parameterization for Estimating Effective Atmospheric Emissivity for Use in Calculating Daytime Downwelling Longwave Radiation. Journal of Applied Meteorology, 38, 474-480. https://doi.org/10.1175/1520-0450(1999)038<0474:Aipfee>2.0.Co;2

https://doi.org/10.5194/egusphere-2023-451
Preprint. Discussion started: 24 April 2023

Chen, M., W. Shi, P. Xie, V. B. S. Silva, V E. Kousky, R. Wayne Higgins, and J. E. Janowiak (2008), Assessing objective techniques for gauge-based analyses of global daily precipitation, J. Geophys. Res., 113, D04110, >), https://doi.org/10.1029/2007JD009132.

CPC Global Unified Temperature. Available online: https://psl.noaa.gov/data/gridded/data.cpc.globaltemp.html, provided by the NOAA PSL, Boulder, Colorado, USA, from their website at https://psl.noaa.gov (accessed on 6 March 2022).

CPC Global Unified Gauge-Based Analysis of Daily Precipitation. Available online: https://psl.noaa.gov/data/gridded/data.cpc.globalprecip.html, provided by the NOAA PSL, Boulder, Colorado, USA, from their website at https://psl.noaa.gov (accessed on 5 March 2022)

Du, M., Kleidon, A., Sun, F., Renner, M., & Liu, W. (2020). Stronger global warming on nonrainy days in observations from China. Journal of Geophysical Research: Atmospheres, 125, e2019JD031792. https://doi.org/10.1029/2019JD031792

Doelling, D. R., Loeb, N. G., Keyes, D. F., Nordeen, M. L., Morstad, D., Nguyen, C., and Sun, M.: Geostationary enhanced temporal interpolation for CERES flux products, J. Atmos. Ocean. Tech., 30, 1072–1090, 2013.

Doelling, D. R., Sun, M., Nguyen, L. T., Nordeen, M. L., Haney, C. O., Keyes, D. F., and Mlynczak, P. E.: Advances in geostationary-derived longwave fluxes for the CERES synoptic (SYN1 deg) product, J. Atmos. Ocean. Tech., 33, 503–521, 2016.

Duarte, H. F., N. L. Dias, and S. R. Maggiotto, 2006: Assessing daytime downward longwave radiation estimates for clear and cloudy skies in Southern Brazil. *Agricultural and Forest Meteorology*, **139,** 171-181. https://doi.org/10.1016/j.agrformet.2006.06.008

Flerchinger, G. N., W. Xaio, D. Marks, T. J. Sauer, and Q. Yu, 2009: Comparison of algorithms for incoming atmospheric long-wave radiation. *Water Resources Research*, **45**. https://doi.org/10.1029/2008WR007394

Hatfield, J. L., R. J. Reginato, and S. B. Idso, 1983: Comparison of long-wave radiation calculation methods over the United States. *Water Resources Research*, **19,** 285-288. https://doi.org/10.1029/WR019i001p00285

Held, I. M., and B. J. Soden, 2000: Water Vapor Feedback and Global Warming. Annual Review of Energy and the Environment, 25, 441-475.

Hersbach, H., and Coauthors, 2018: ERA5 hourly data on single levels from 1959 to present. Copernicus Climate Change Service (C3S) Climate Data Store (CDS). (Accessed on < 06-03-2022 >), https://doi.org/10.24381/cds.adbb2d47 .

Kato, S., Rose, F. G., Rutan, D. A., Thorsen, T. E., Loeb, N. G., Doelling, D. R., Huang, X., Smith, W. L., Su, W., and Ham, S.-H.: Surface irradiances of Edition 4.0 Clouds and the Earth's Radiant Energy System (CERES) Energy Balanced and Filled (EBAF) data product, J. Climate, 31, 4501–4527, https://doi.org/10.1175/JCLI-D-17-0523.1, 2018.

Kleidon, A., and M. Renner, 2017: An explanation for the different climate sensitivities of land and ocean surfaces based on the diurnal cycle. Earth Syst. Dynam., 8, 849-864. https://doi.org/10.5194/esd-8-849-2017

Lee, S., T. Gong, S. B. Feldstein, J. A. Screen, and I. Simmonds, 2017: Revisiting the Cause of the 1989–2009 Arctic Surface Warming Using the Surface Energy Budget: Downward Infrared Radiation Dominates the Surface Fluxes. Geophysical Research Letters, 44, 10,654-610,661. https://doi.org/10.1002/2017GL075375.

Loeb, N. G., Doelling, D. R., Wang, H., Su, W., Nguyen, C., Corbett, J. G., Liang, L., Mitrescu, C., Rose, F. G., and Kato, S.: Clouds and the Earth's Radiant Energy System (CERES) Energy Balanced and Filled (EBAF) Top-of-Atmosphere (TOA) Edition-4.0 data product, J. Climate, 31, 895–918, https://doi.org/10.1175/JCLI-D-17-0208.1, 2018.

Esmael Malek, 1997. Evaluation of effective atmospheric emissivity and parameterization of cloud at local scale. Atmospheric Research, 45 (1), 41-54, https://doi.org/10.1016/S0169-8095(97)00020-3 .

Monteith, J.L. and Unsworth, M.H. (2008) Principles of Environmental Physics. 3rd Edition, Academic Press, New York, 418.

NASA/LARC/SD/ASDC. (2017). CERES and GEO-Enhanced TOA, Within-Atmosphere and Surface Fluxes, Clouds and Aerosols Monthly Terra-Aqua Edition4A [Data set]. NASA Langley Atmospheric Science Data Center DAAC. (Accessed on < 09-03-2022 >), https://doi.org/10.5067/TERRA+AQUA/CERES/SYN1DEGMONTH_L3.004A.

Park, H.-S., S. Lee, S.-W. Son, S. B. Feldstein, and Y. Kosaka, 2015: The impact of poleward moisture and sensible heat flux on Arctic winter sea ice variability. J. Climate, 28, 5030–5040, https://doi.org/10.1175/JCLI-D-15-0074.1

https://doi.org/10.5194/egusphere-2023-451
Preprint. Discussion started: 24 April 2023

Pastorello, G., and Coauthors, 2020: The FLUXNET2015 dataset and the ONEFlux processing pipeline for eddy covariance data. Scientific Data, 7, 225. https://doi.org/10.1038/s41597-020-0534-3

Sridhar V, Ronald L Elliott, 2022: On the development of a simple downwelling longwave radiation scheme, Agricultural and Forest Meteorology, 112, 3–4, 237-243, https://doi.org/10.1016/S0168-1923(02)00129-6.

Satterlund, D. R., 1979: An improved equation for estimating long-wave radiation from the atmosphere. Water Resources Research, 15, 1649-1650. https://doi.org/10.1029/WR015i006p01649

Su, J., A. Duan, and H. Xu, 2017: Quantitative analysis of surface warming amplification over the Tibetan Plateau after the late 1990s using surface energy balance equation. Atmospheric Science Letters, 18, 112-117. https://doi.org/10.1002/asl.732

Tian, Y., Zhang, Y., Zhong, D., Zhang, M., Li, T., Xie, D., & Wang, G. (2022). Atmospheric Energy Sources for Winter Sea Ice Variability over the North Barents–Kara Seas, Journal of Climate, 35(16), 5379-5398. https://doi.org/10.1175/JCLI-D-21-0652.1

Trenberth, K. E., Fasullo, J. T., & Kiehl, J. (2009). Earth's Global Energy Budget, *Bulletin of the American Meteorological Society*, *90*(3), 311-324. https://doi.org/10.1175/2008BAMS2634.1

Monteith, J.L., and Unsworth, M.H. 2008. Principles of Environmental Physics. Third Ed. AP, Amsterdam. http://store.elsevier.com/Principles-of-Environmental-Physics/John-Monteith/isbn-9780080924793/.

UNCOD Secretariat (1977) Desertification: Its causes and consequences, Pergamon Press, 448 p.

Wang, K., and S. Liang, 2009: Global atmospheric downward longwave radiation over land surface under all-sky conditions from 1973 to 2008. *Journal of Geophysical Research: Atmospheres*, **114**. https://doi.org/10.1029/2009JD011800

Wei, Y., and Coauthors, 2021: Trends and Variability of Atmospheric Downward Longwave Radiation Over China From 1958 to 2015. *Earth and Space Science*, **8,** e2020EA001370. https://doi.org/10.1029/2020EA001370

Xie, P., Chen, M., Yang, S., Yatagai, A., Hayasaka, T., Fukushima, Y., & Liu, C. (2007). A Gauge-Based Analysis of Daily Precipitation over East Asia, Journal of Hydrometeorology, 8(3), 607-626. https://doi.org/10.1175/JHM583.1.

Zampieri, M., F. D'Andrea, R. Vautard, P. Ciais, N. de Noblet-Ducoudré, and P. Yiou, 2009: Hot European Summers and the Role of Soil Moisture in the Propagation of Mediterranean Drought. *Journal of Climate*, **22,** 4747-4758. https://doi.org/10.1175/2009JCLI2568.1

Figures

https://doi.org/10.5194/egusphere-2023-451
Preprint. Discussion started: 24 April 2023

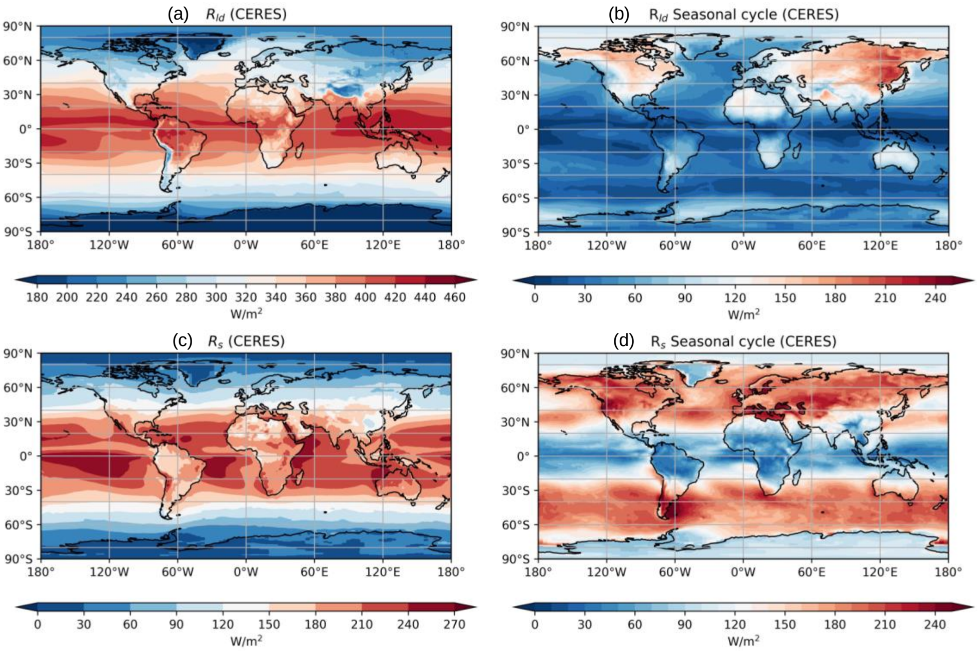

Figure 1. Spatial distribution of (a, c) the climatological mean and (b, d) the seasonal amplitude of downward longwave radiation and absorbed solar radiation at the surface respectively from the NASA-CERES dataset. The seasonal amplitude is calculated as the difference between the maximum and minimum monthly mean.

https://doi.org/10.5194/egusphere-2023-451
Preprint. Discussion started: 24 April 2023

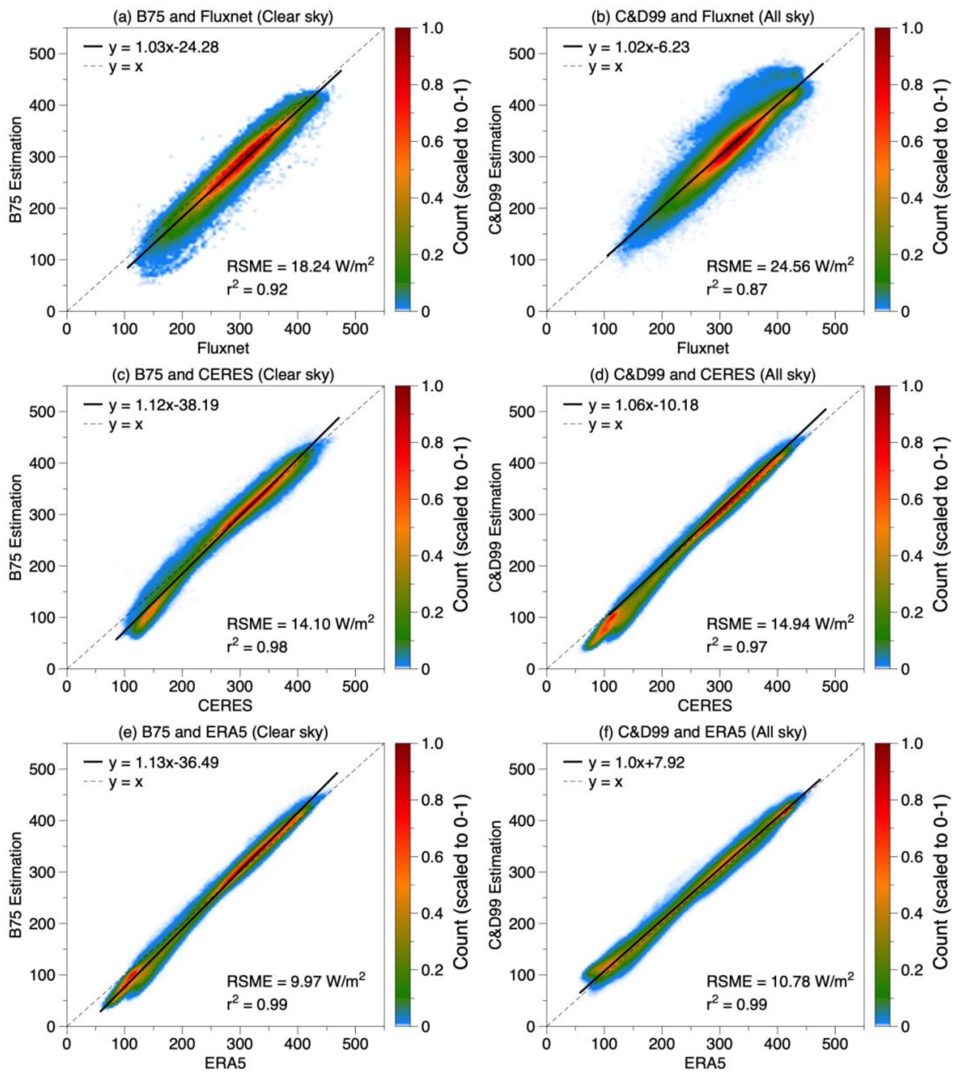

Figure 2. Comparison of R_{ld} estimated (a, c, e) by Brutsaert (1975) for clear-sky conditions and (b, d, f) by Crawford and Duchon (1999) for all-sky conditions using FLUXNET (a, b), NASA-CERES (c, d) and ERA5 (e, f). Colors indicate the density of the data points and is scaled to values between 0 - 1.

https://doi.org/10.5194/egusphere-2023-451
Preprint. Discussion started: 24 April 2023

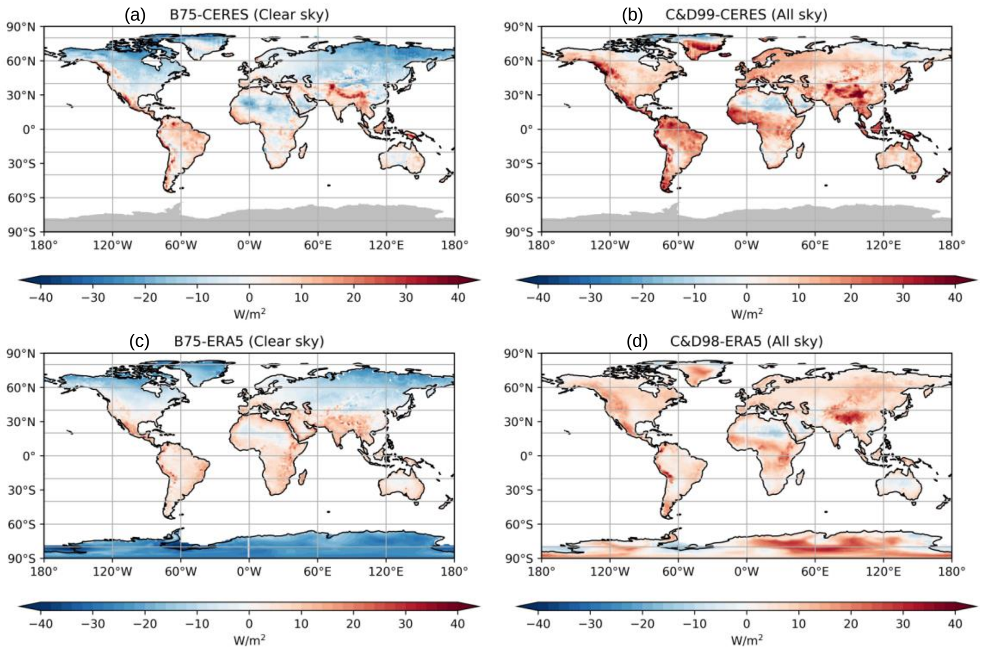

380

381 **Figure 3.** Biases in the estimates for R_{ld} for (a, b) NASA-CERES and (c, d) ERA reanalysis for (a, c) clear-
382 sky and (b, d) all-sky conditions over land. Grey shading indicate missing values.
383

https://doi.org/10.5194/egusphere-2023-451
Preprint. Discussion started: 24 April 2023

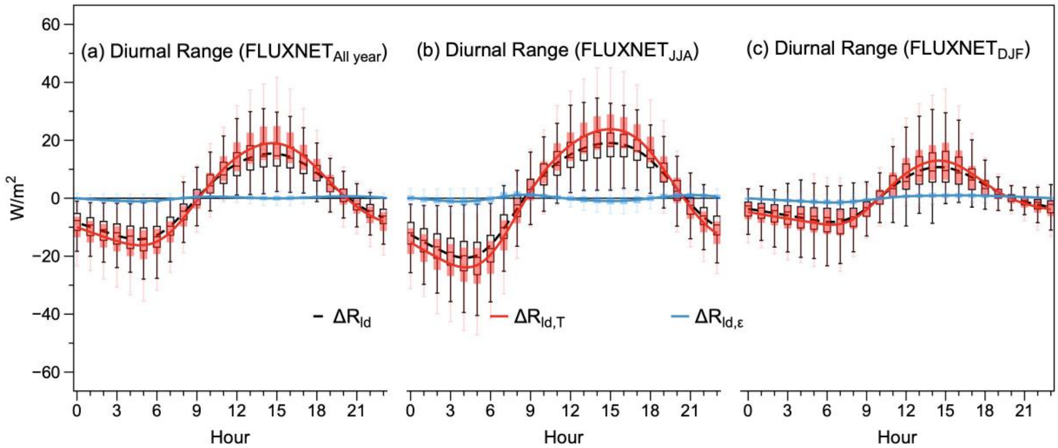

Figure 4. Diurnal variations in R_{ld} (black dashed line) and its decomposition into contributions by changes in emissivity (blue, $\Delta R_{ld,\varepsilon}$) and atmospheric heat storage (red, $\Delta R_{ld,T}$) in the FLUXNET dataset aggregated over 189 sites for (a) the whole year, (b) June-August, and (c) December - February. The upper and lower whisker indicate 95th and 5th percentiles, upper boundary, median line, and lower boundary of the box indicate the 75th, 50th, 25th quantiles, respectively. Regression lines are based on site-mean or grid-mean value using LOESS regression.

https://doi.org/10.5194/egusphere-2023-451
Preprint. Discussion started: 24 April 2023

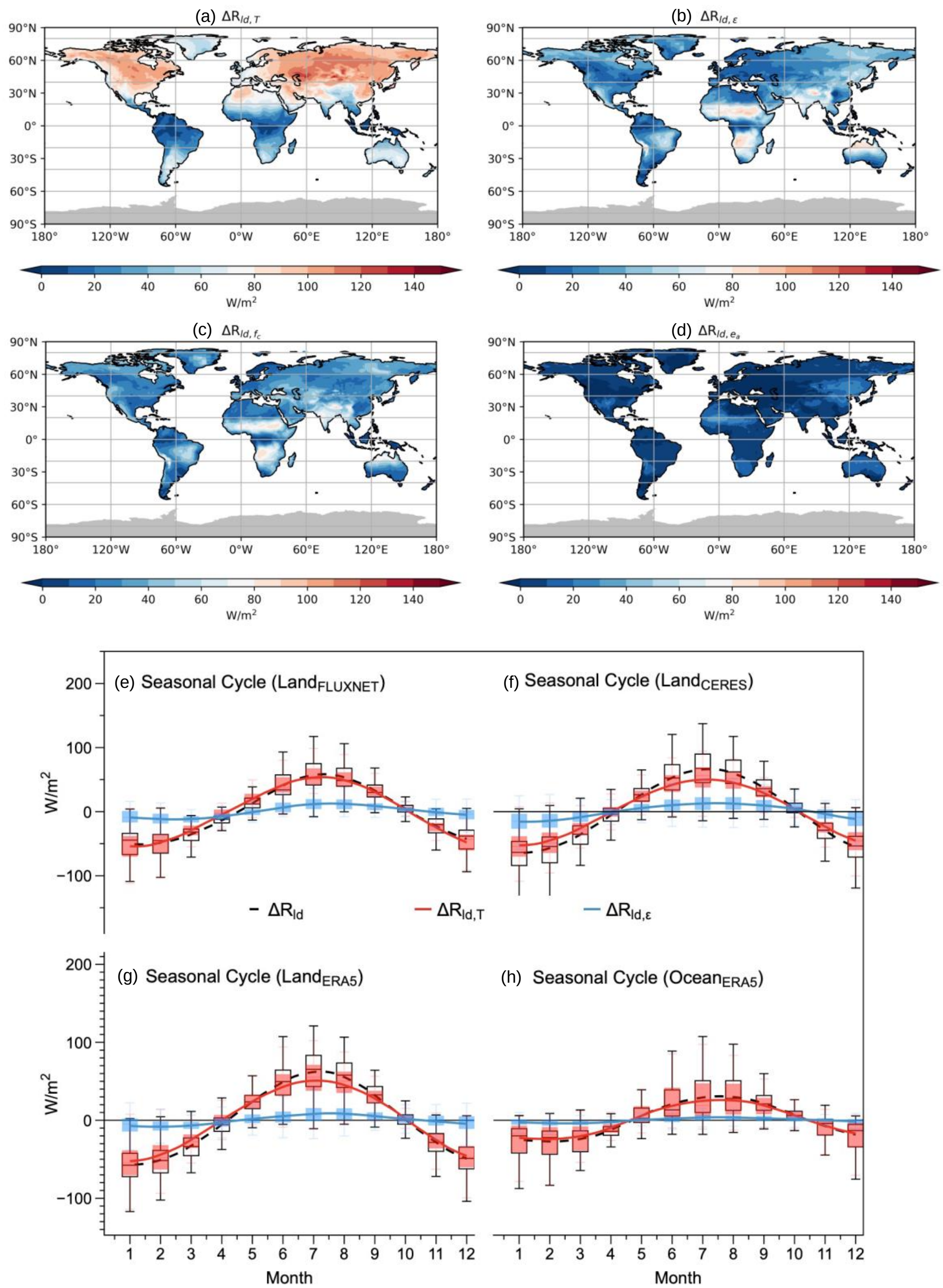

392

https://doi.org/10.5194/egusphere-2023-451
Preprint. Discussion started: 24 April 2023

Figure 5. Decompositions of the mean seasonal variation of R_{ld} (difference between the maximum and minimum monthly means) in the NASA-CERES dataset into contributions by (a) atmospheric heat storage ($\Delta R_{ld,T}$) and (b) emissivity ($\Delta R_{ld,\varepsilon}$). The variations in $\Delta R_{ld,\varepsilon}$ are further decomposed in contributions by variations in (c) cloud cover ($\Delta R_{ld,f_c}$) and (d) humidity ($\Delta R_{ld,e_a}$). Panels (e) - (h) show the mean seasonal variation of R_{ld} averaged over land or ocean and its decomposition into variations in atmospheric heat storage ($\Delta R_{ld,T}$) and emissivity ($\Delta R_{ld,\varepsilon}$) using FLUXNET, NASA-CERES, and ERA5. The box plot indicates percentiles and quantiles as in Figure 4. Grey shading indicates missing values.

https://doi.org/10.5194/egusphere-2023-451
Preprint. Discussion started: 24 April 2023

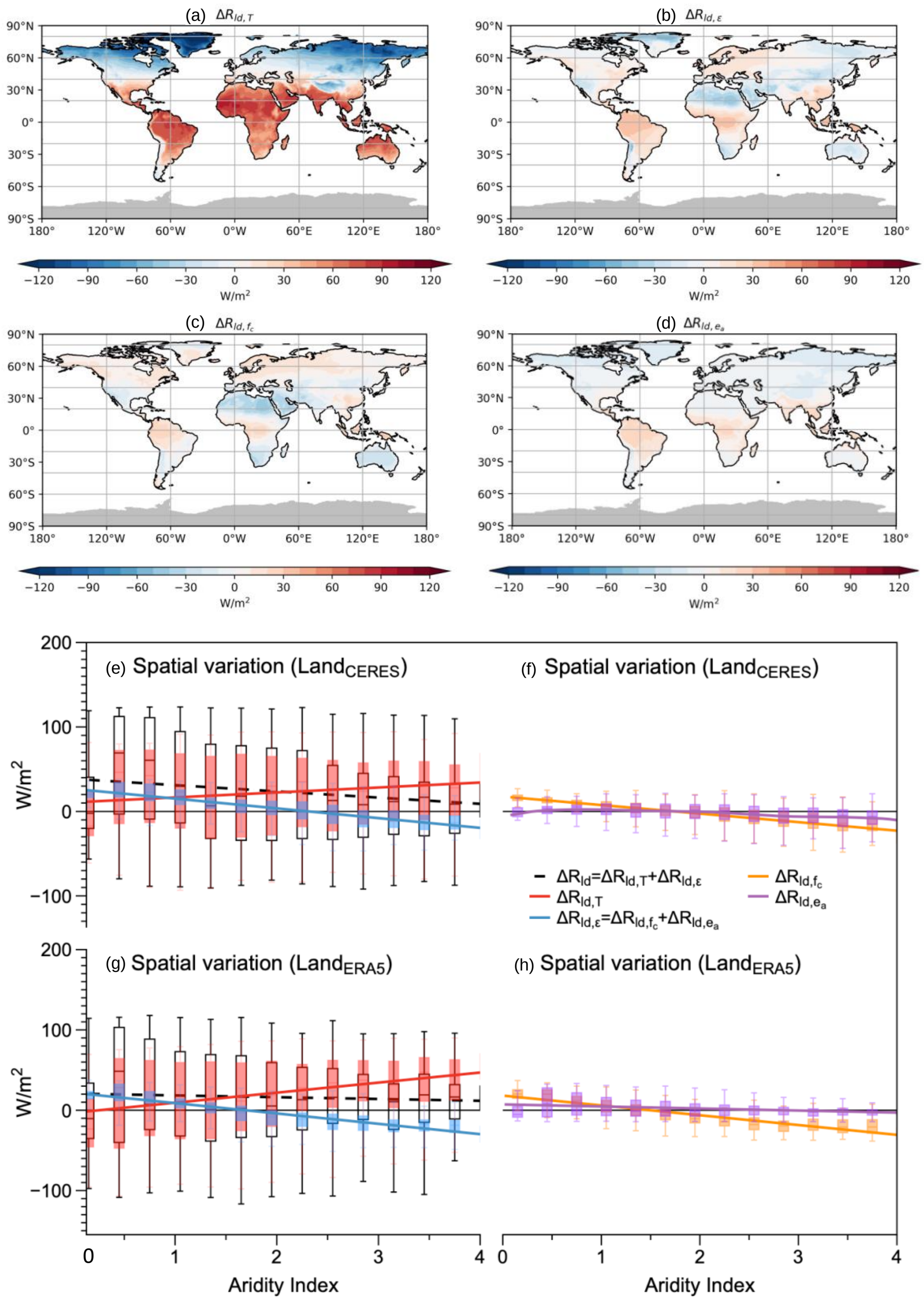

https://doi.org/10.5194/egusphere-2023-451
Preprint. Discussion started: 24 April 2023

Figure 6. As Figure 5, but for the decomposition of the spatial variations of the annual mean (a - d) and the variations with the aridity index (e - h).

Plain Language:

Downward longwave radiation (R_{ld}) plays an important role in surface energy balance and is critical for global warming. However, its spatiotemporal climatological variation on a global scale has not been explained well with a solid physical basis. To fill this gap, we here use a semi-empirical equation derived by Brutsaert (1975, "B75") and its extension by Crawford and Duchon (1999, "C&D99") to identify the leading terms responsible for the diurnal range, seasonal cycle, and geographical variations in R_{ld}. We show that B75 and C&D99 work very well when evaluated against global observations from satellites and FLUXNET sites. We then used these physics-based equations to show that diurnal and seasonal variations in R_{ld} are predominantly controlled by changes in atmospheric heat storage. When moving from humid to arid regions, while the contribution of atmospheric heat storage increases, the ones from clouds decreases, which together explains the relatively small decrease in R_{ld} with aridity. Our work provides a clue to better understand aspects of climate variability, extreme events, and global warming, by linking these to the mechanistic contributions by downwelling longwave radiation.